ENFOQUE UTE
REVISTA
Facultad Ciencias de la Ingeniería e Industrias

RESEARCH ARTICLE

ENFOQUE UTE, VOL. 17, NO. 1, pp. 34-42, E-ISSN: 1390-6542
RECEIVED JULY 25, 2025; REVISED OCTOBER 20, 2025; ACCEPTED OCTOBER 30, 2025; PUBLISHED ONLINE DECEMBER 20, 2025; PUBLICATION DATE JANUARY 1, 2026.

Citation: J. Toapaxi Álvarez, R. Sandoval Garzón, K. Soto Morales, and C. Torres Jacobowitz, "Hydrodynamic Analysis of Special Shaped Submerged Panels in Curved Channels Using Three-Dimensional Numerical Modelling," Enfoque UTE, vol. 17, no. 1, pp. 34-42, Jan. 2026, doi: https://doi.org/10.29019/enfoqueute.1216

Hydrodynamic Analysis of Special Shaped Submerged Panels in Curved Channels Using Three-Dimensional Numerical Modelling

Jorge Toapaxi Álvarez[1], Ricardo Sandoval Garzón[2*], Karen Soto Morales[3], Cristina Torres Jacobowitz[4]

***Abstract* — This paper analyses the water flow in curved channels, which may present particular hydrodynamic patterns such as streamline alteration, cross-wave formation, recirculation zones and possible contour flow separations, all of which require detailed hydrodynamic analysis. The analysis focuses on a case study of a hydroelectric power plant intake with a side grate, which includes a curved (small-radius) gravel-removing channel connecting the intake works to two desanding chambers. This design results in an unequal distribution of flow to the desanding chambers, causing neither chamber to function properly, and a recirculation zone upstream of the left desanding chamber.**

The methodology uses three-dimensional numerical modelling in OpenFOAM, based on prototype data. The model was calibrated with a flow rate of 8,8 m³/s. Subsequently, the transit of the design flow of 13 m³/s was simulated and an uneven flow distribution in the desanding chambers was verified. To address this problem, and considering the higher-velocity streamlines, two groups of alternatives were considered: the first consisted of placing two panels of different special shapes (straight, broken, and curved) in the desilting chamber; the second examined the flow behavior with an increased number of panels and alteration aspect ratio.

For the first group, the scenarios tested did not modify the flow distribution in the sand removal chambers; however, the panels locally changed the hydrodynamic conditions and successfully altered the recirculation zone location. The scenarios in the second group yielded the best operational results regarding flow distribution.

***Keywords:* CFD; OpenFOAM; streamlines; optimization.**

***Resumen* — El presente trabajo analiza el flujo de agua en canales curvos, que pueden presentar patrones hidrodinámicos particulares, como la alteración de las líneas de corriente, formación de ondas cruzadas, zonas de recirculación y posibles separaciones de flujo en los contornos; todos ellos requieren un análisis hidrodinámico detallado. El análisis se centra en un caso de estudio de una obra de toma con reja lateral de una central hidroeléctrica, que incluye un desripiador de canal curvo y radio pequeño, que conecta la obra de toma a dos cámaras desarenadoras. Este diseño origina una distribución inequitativa del caudal hacia las cámaras desarenadoras, ocasionando que ninguna funcione adecuadamente, y genera una zona de recirculación aguas arriba de la cámara desarenadora izquierda.**

La metodología emplea modelización numérica tridimensional en OpenFOAM, basada en datos de prototipo. El modelo fue calibrado con un caudal de 8,8 m³/s. Posteriormente, se simuló el tránsito del caudal de diseño de 13 m³/s y se verificó una distribución desigual de caudales en las cámaras desarenadoras. Para abordar este problema, considerando las líneas de corriente de mayor velocidad, se evaluaron dos grupos de alternativas: el primero consistió en ubicar en el desripiador dos paneles de diferentes formas especiales en planta (rectos, quebrados y curvos), y el segundo verificó el comportamiento del flujo con un aumento en el número de paneles y la alteración de la relación de aspecto.

En el primer grupo, los escenarios ensayados no modificaron la distribución de caudales en las cámaras desarenadoras. Sin embargo, los paneles modificaron localmente las condiciones hidrodinámicas y lograron alterar la ubicación de la zona de recirculación identificada. Los escenarios del segundo grupo fueron los que arrojaron mejores resultados operativos en cuanto a la distribución de caudales.

***Palabras Clave:* CFD; OpenFOAM; líneas de corriente; optimización.**

I. INTRODUCTION

In an open channel bend, the flow pattern changes as a result of the presence of centrifugal force [1], and a particularly due to the curvature ratio (bend radius over channel width,

Authors acknowledge the support provided by Escuela Politécnica Nacional.

* *Corresponding author:* ricardo.sandoval@epn.edu.ec.

1. Jorge Toapaxi Álvarez is with Centro de Investigaciones y Estudios de Ingeniería de los Recursos Hídricos & Departamento de Ingeniería Civil y Ambiental at Escuela Politécnica Nacional, Quito 170517, Ecuador. E-mail: jorge.toapaxi@epn.edu.ec. ORCID number https://orcid.org/0000-0003-1344-5159.
2. Ricardo Sandoval Garzón is with Centro de Investigaciones y Estudios de Ingeniería de los Recursos Hídricos & Departamento de Ingeniería Civil y Ambiental at Escuela Politécnica Nacional, Quito 170517, Ecuador. E-mail: ricardo.sandoval@epn.edu.ec. ORCID number https://orcid.org/0000-0002-6867-0196.
3. Karen Soto Morales is with Facultad de Ingeniería Civil y Ambiental at Escuela Politécnica Nacional, Quito 170517, Ecuador. E-mail: karen.soto@epn.edu.ec. ORCID number https://orcid.org/0009-0008-9550-3853.
4. Cristina Torres Jacobowitz is with Centro de Investigaciones y Estudios de Ingeniería de los Recursos Hídricos & Departamento de Ingeniería Civil y Ambiental at Escuela Politécnica Nacional, Quito 170517, Ecuador. E-mail: cristina.torresj@epn.edu.ec. ORCID number https://orcid.org/0000-0001-9639-6668.

DOI: https://doi.org/10.29019/enfoqueute.1216
***Associate Editor:** Marcelo Mosquera*

R/B) and aspect ratio (channel width over water depth, B/H) [2]. Thes most typical feature is the presence of secondary currents that depend on turbulence [3] and have affect bottom topography and riverbanks [4].

Simplified two-dimensional models have produced accurate predictions for flow in channels of gentle to moderate curvature, but not in highly curved channels. Three-dimensional (3D) Reynolds-Averaged Navier-Stokes (RANS) numerical models have made it possible to investigate flow and sediment transport in medium- and high- curvature channels; however, they have not been able to reproduce some finer details. According to [5] and [3] a higher-order turbulence model such as a Reynolds Stress model (RSM) or a Large Eddy Simulation (LES) is required to predict features such as the secondary counter-rotating cell on the outer bank. However, LES-type approaches are computationally expensive. Among the most widely used software programs is the open-source OpenFOAM, as shown in [6].

To modify the flow pattern in rivers, [7] suggests implementing structures known as submerged panels to control sediment movement in the cross-section and prevent bank erosion. The structures are installed with a deflection angle relative to the flow direction (Fig. 1), generating a secondary helical flow that alters the magnitude and direction of shear stresses on the bed and causes changes in velocity distribution, water depth and sediment transport. Generally, the panels are installed in rows along the outer banks of river bends, in long stretches, to generate large vortices that influence the overall flow pattern. According to [8], the transverse spacing between panels in a row should be carefully selected so that the separated vortices can merge and form the helical flow.

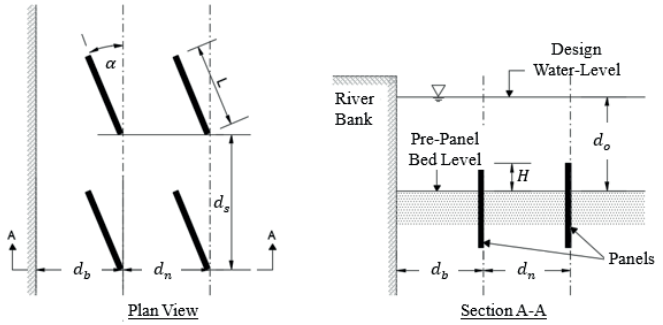

Fig. 1. Submerged panels design parameters.

Several works analyze the effect of installing submerged flat panels, considering different attack angles and arrangements [9], and the height and length variations in narrow and highly curved channels [10]. Likewise, other panel shapes —broken, angular and curved— have also been studied ([11]; [12]).

The present research focuses on the hydrodynamic analysis of submerged panels in curved fixed-bottom channels using three-dimensional numerical modeling with the open-source Computational Fluid Dynamics (CFD) program Open Source Field Operation and Manipulation (OpenFOAM), which employs the Finite Volume Method (FVM) to solve the governing equations of fluid mechanics, considering the principles of conservation of mass, momentum and energy [13]. Version 2312 of OpenFOAM was used under the Linux Ubuntu operating system.

This study considers the intake works of a hydroelectric power plant located in Ecuador, which presents a problem in flow distribution to the desanding chambers due to the curved geometry of the desripper. As a result, the flow is not equitably divided between the desanding chambers, generating inefficiencies in the sedimentation process and posing risks to the generation units due to sediment entry into the load tank. With information from the "AS BUILT" plans (Fig. 2) and field data, the OpenFOAM numerical model was applied.

TABLE I
DESIGN TYPICAL DIMENSIONS

Variable	Dimension
Design water depth, d_o	
Panel height, h	0,2–04 d_o
Panel thickness	0,05–0,20 m
Panel length, L	3h
Lateral spacing, d_n	3h
Longitudinal spacing, d_s	10–30h
Distance up to bank, d_b	3h
Attack angle, α	10–20 *degrees*

Using the configuration of an actual structure allows for the evaluation of submerged-panel design recommendations (Table I) applied to a curved channel with a small radius of curvature, with the aim of mitigating undesirable hydraulic phenomena such as cross-flow or recirculation zones, thus allowing for validation or suggestion of new compositions depending on the overall purpose of the structure.

II. MATERIALS AND METHODS

A. Study case description

The hydroelectric plant has a 13 m^3/s design flow. The intake consists of 4 lateral racks, each with a 3,15 m base section by 2,0 m height; a curved-wall screen with a 132° turning angle, which connects to a two-chamber desander (each 8,20 m wide and 32 m long); and transition structures that reach a length of approximately 58 m, until they join the 3,0-m-wide and 3,5-km-long open conduction channel. Once the flow reaches the surge tank, it is conveyed for hydroelectric generation through a steel pressure pipe. The intake of the hydroelectric plant is shown in Fig. 2.

Due to flow inertia entering through the racks and the 132° turning angle, the incoming flow does not achieve equal distribution between the desanding chambers (i.e., 6,5 m^3/s each). The right chamber receives a higher flow, reducing its sediment-retention efficiency. According to design criteria in [14] and [15], sedimentation processes in the right chamber are

affected due to the inlet-zone geometry (curve), which produces high velocities, dead zones, and turbulence.

During the field visit, liquid-flow gauging was performed using the velocity and cross-sectional area method. Water-level measurements were also taken at weirs for calibration and validation of the numerical model.

The operation of the hydroelectric plant has shown that sediments have even reached the powerhouse, indicating that the protective structures are not functioning properly.

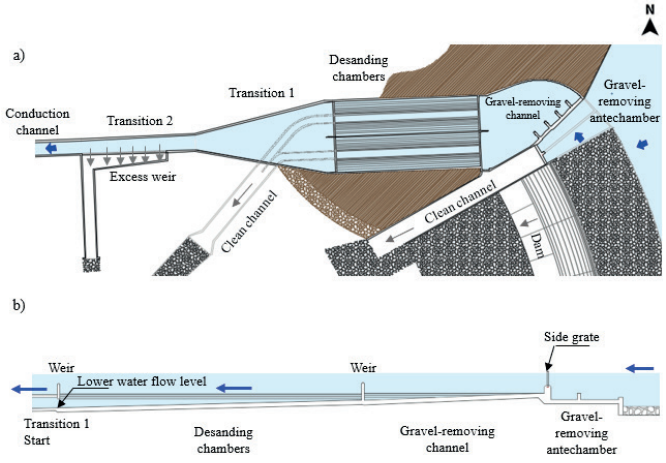

Fig. 2. Study case water intake schemes: a) plan view, and b) flow profile.

B. Base numerical model

Computational Fluid Dynamics (CFD) is a technique that uses high-performance computing equipment and numerical methods to solve physical problems related to fluid motion [16]. The method allows optimizing time and economic resources compared with physical models. In this context, several scenarios were simulated using different shapes and arrangements of submerged panels, aiming to generate recommendations to achieve an equitable flow distribution in the desanders (Fig. 3). For this purpose, OpenFOAM software and two computers were used.

Fig. 3. Analyzed hydraulic structures prototype.

The turbulence model selected was k-ω SST, due to computational limitations that prevented the use of the LRR model, which provides a better representation of flow-separation phenomena and highly curved streamlines. However, in velocity-profile and pressure-domain analyses in curved structures, the k-ω SST model has shown reliable results [17].

The interFoam solver, designed for two-phase air-water phenomena, was used. Numerical stability was controlled by setting a variable time step based on a maximum CFL value of 0,85.

The numerical-stability results of the model are presented using graphs showing flow variation over time at the inlet and outlet, as shown in Fig. 8.

1) Geometry and meshing

Based on the "AS BUILT" drawings, the computational domain of the model was identified, consisting only of the internal volume occupied by the fluid. It includes:

i) The flow inlet zone.
ii) Desripper antechamber.
iii) Desripper.
iv) Desanding chambers.
v) The outlet transition.

The computational domain (Fig. 4) was configured using a structured base mesh generated with OpenFOAM's native blockMesh function, with a hexahedral block scheme. The base block level was set at the lowest elevation of the flow domain (8,55 m), and the reference elevation of the water-air interface was set at the grid's upper level at the scrapper inlet (12,58 m).

An approximate mesh size of 20 cm was achieved for the three Cartesian axes. The incorporation and refinement of the base mesh, as well as the inclusion of the panel geometry, were carried out using snappyHexMesh, based on triangular discretization STL files. The three-dimensional modeling of the special shapes was performed in FreeCAD, and MeshLab was used as a reader for visualization in the OpenFOAM environment.

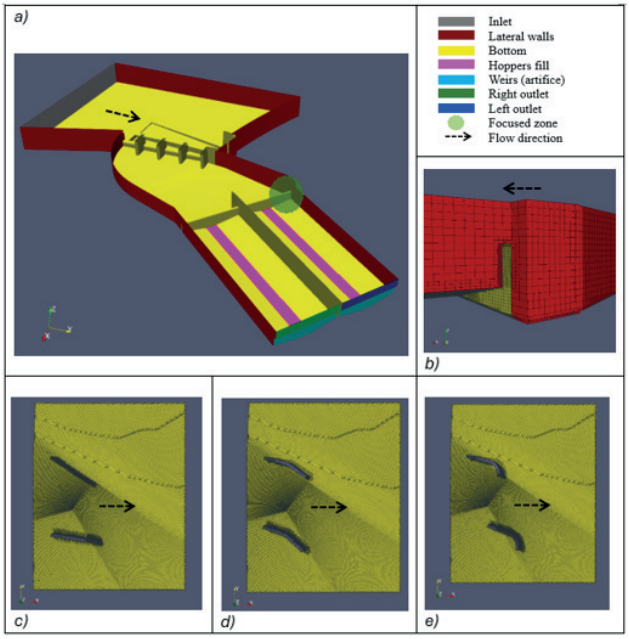

Fig. 4. a) Computational domain perspective; b) structured mesh detail and special-area coupling; meshing details: c) flat; d) broken, and e) curved.

2) Initial and boundary conditions

All boundary conditions describe the behavior of a hydrodynamic phenomenon at the free surface and are based on recommendations from similar studies in open channels [18].

A Newtonian, incompressible, two-phase air-water flow was considered. In the "transportProperties" file, the essential properties —kinematic viscosity and density of both fluids —were defined.

To reduce simulation time, an initial water volume up to elevation 12,06 m was included in the domain using the "boxToCell" functionality of the "setFields" file. This ensures wet-initial conditions and prevents adverse effects such as strong velocity gradients resulting from filling processes in chambers bounded by internal control structures (spillways) that make up the overall configuration of the model.

For the water-air interface (alpha.water), the inlet assumed a "variableHeightFlowRate" condition, which delimits the inlet level at a height of 0 to 3,85 m. Walls and outlet used "zeroGradient" condition, and the atmospheric boundary used "inletOutlet".

For velocity management in the model, the following configuration was established: the use of the "variableHeightFlowRateInletVelocity" condition with a value of (cal: 8,8 m^3/s; val: 13,00 m^3/s) at the inlet; for the rigid contours (walls) a "fixedValue" type; for the atmospheric zone the 'pressureInletOutletVelocity' condition; and for both outlets of the model (disanding chambers) a free discharge of the "inletOutlet" type for the validation process and, "outletPhaseMeanVelocity" with 1,56 (m/s) for calibration model.

In the pressure management section, the grouping is executed by following: the atmospheric layer with the "totalPressure" type condition; inlet and outlet with "zeroGradient", and walls the condition "fixedFluxPressure" was assigned. For validation model, inlet and outlets were changed to "fixedFluxPressure".

Roughness was defined in the nut file using "nutkRoughWallFunction" for the walls. For the rest of the inlet, outlet, and atmosphere patches, the condition "calculated" was chosen.

C. Calibration

The calibration process was carried out using four structured base blocks, defining regular hexahedrons measuring 60, 40, 20, and 15 cm. The overall refinement and curvature levels for configuring the bottom geometry with its characteristics (inlet racks, weirs, bottom slopes, etc.) were defined for all cases as 1 and 3, respectively. In addition, the sharp angle and flat angle resolution values were 40 and 30 degrees, respectively. Finally, an explicit refinement level of zero was established for the edges of the features. Fig. 5 shows the result of the refinement process achieved with the snappyHexMesh algorithm.

The model calibration was performed by modifying the roughness values. Field data were entered corresponding to a flow rate lower than the design flow rate (8.8 m^3/s) and a water depth at the crest of the outlet weirs of the desanding chambers of about 0,77 m.

As a first value of Manning's roughness, 0,015 was taken, which corresponds to concrete in open channels, as shown in Table II [19].

TABLE II
MANNING'S COEFFICIENTS FOR OPEN CHANNELS

Flume type	Manning (n)	Range
Coated channels:		
Brick, plastered	0,013	0,011-0,015
Brick	-	0,012-0,018
Concrete, smoothed	0,015	0,011-0,020

In OpenFOAM, the roughness must be entered in terms of absolute roughness; therefore, Eq. (1) is used:

$$n = \frac{D50^{\frac{1}{6}}}{25,6} \quad (1)$$

Where *n* represents Manning's roughness coefficient and D_{50} is the absolute roughness in meters.

Strickler's (1923) equation can be used, under the assumption that the flow is completely turbulent, to estimate the roughness factor of channels and rivers as a function of the predominant sediment sizes [19].

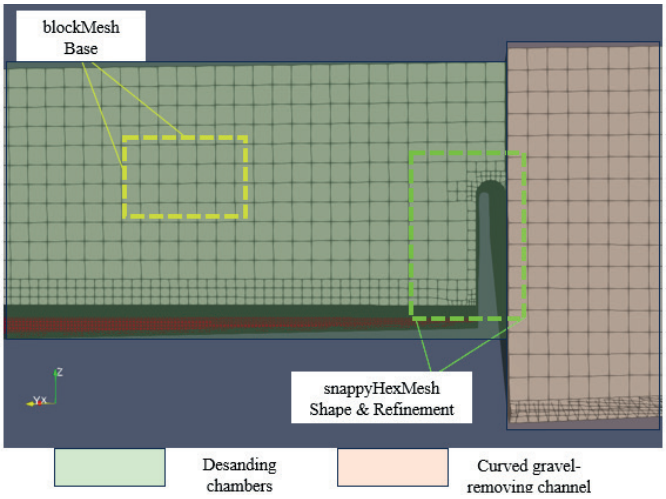

Fig. 5. Mesh refinement detail for wall-like contours.

Therefore, using Eq. (1), the starting point for the roughness coefficient is 3,3 mm. To calibrate the numerical model, values corresponding to the ranges for *"n"* of Manning's concrete in open channels were used, considering a uniform distribution across the entire rough bottom of the model; that is, no roughness zoning was applied. This was due to the presence of sediment throughout the established domain, given the ineffectiveness of the disbanding chambers, which allow sediment to pass through even to the powerhouse.

Finally, the calibration of the model is achieved with a Manning's coefficient of 0,018, which corresponds to an absolute roughness of 9,6 mm, meeting 92 % continuity and water depth at the outlet crest of the weirs (field data) with approximately 90 % accuracy.

The mesh convergence index, with respect to water depth-field value on the right outlet spillway desanding chamber (77 cm), for the results of the models obtained at 300 seconds of

simulation, shows that the 20 cm mesh size yields the best results, as can be seen in Fig. 6. It should be noted that for the 15 cm mesh size, a simulation time of 200 seconds was achieved in approximately 13 days of calculation, a performance far below that of the other calibration models.

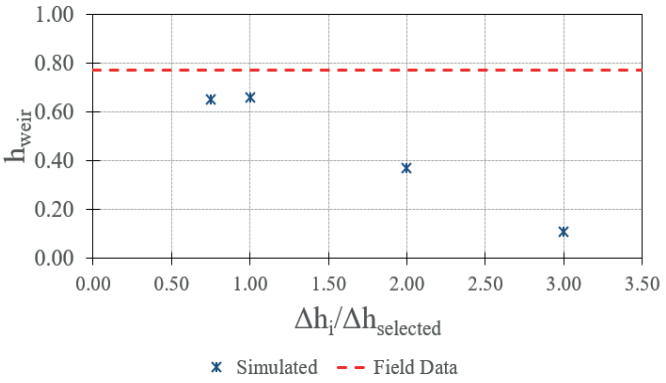

Fig. 6. Grid Convergence Index analysis for water depth over weir crest.

D. Validation

Model validation was performed with the design flow corresponding to 13 m^3/s, and considering a simplification of the geometry to optimize calculation time. The model output is located in the middle of the length of transition 1, whose section has a draft of 2,33 m (validation parameter with its corresponding velocity). This computational domain arrangement is validated by verifying the water depth on the weirs at the inlet of both desanding chambers and based on the results of the calibration model; by incorporating thick-walled weirs at both "artificial" outlets, all with the aim of generating the corresponding upstream control section without altering the behavior in the interest area. The generation of two outlet patches contributes to post-processing for evaluating alternatives in terms of flow redistribution.

The operation of the intake showed inadequate performance, especially in the distribution of flows in the desanding chambers (Fig. 7), since its design intended an almost equal flow distribution, in other words, an operation in which each chamber would receive 6,5 m^3/s under design conditions.

With the calibrated model, based on bottom roughness, mesh size, and evaluation of boundary conditions, validation was carried out considering the design flow rate. The results effectively show a non-uniform distribution of flows entering the desanding chambers: 7,43 m^3/s and 5,54 m^3/s for the right and left chambers, respectively. Compared to the design flow rate of 13 m^3/s, the above values represent 57,29 % and 42,71 % of the total flow obtained at the model outlet (12,97 m^3/s). This value represents 99,78 % with respect to the inlet flow, thus verifying compliance with the principle of continuity in the model.

In the above figure, a preferential high-velocity current is observed towards the right chamber, producing a recirculation zone at the entrance to the left chamber, a phenomenon that can be verified by analyzing the streamlines in that zone.

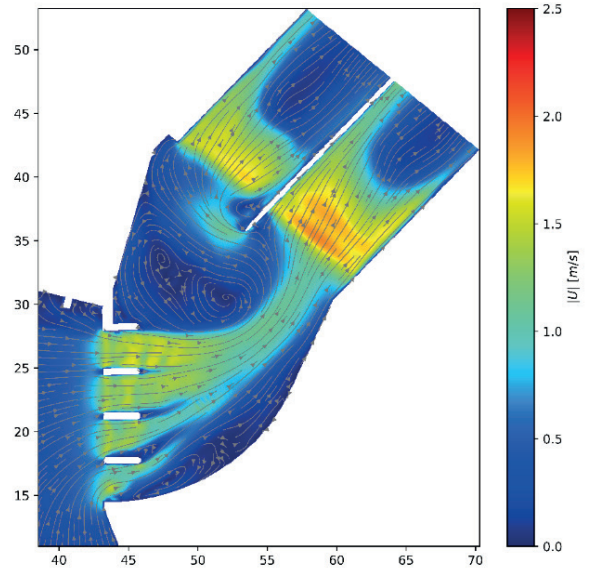

Fig. 7. Numerical model (validation) Q = 13 m^3/s: Velocity distribution (m/s) and streamlines behavior.

In the desanding chambers, the velocity distribution shows greater flow intensity toward the left margins of both chambers, which prevents a stable, slow, and uniform flow that would allow an adequate sedimentation process to occur.

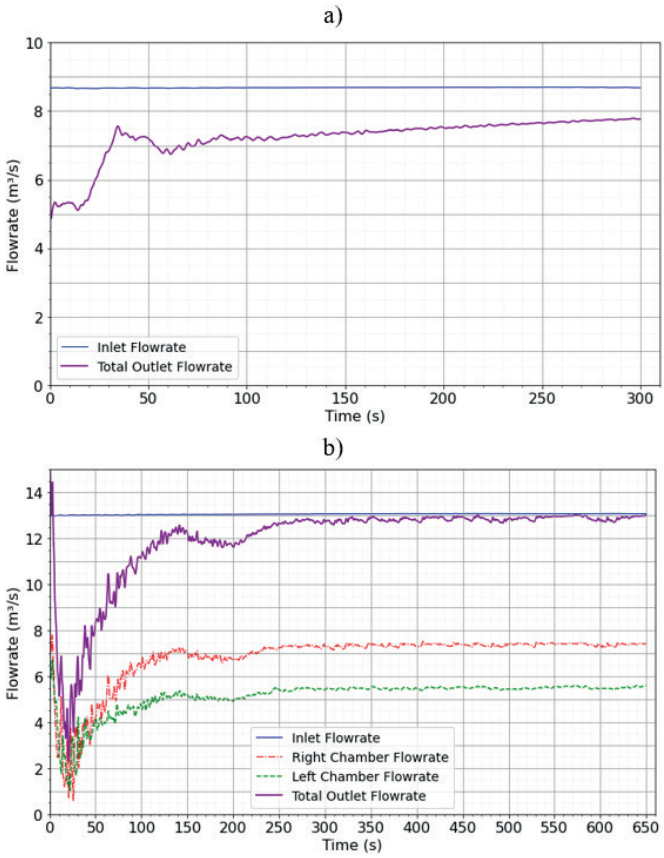

Fig. 8. Hydrograms for models: a) Calibration; b) validation.

E. Simulation scenarios

To stabilize the flow in the desripper, in search of an equitable distribution of flows in the desanding chambers and considering the design flow (13 m^3/s), three alternatives of submerged panels were tested in the first instance, based on the design criteria of [7] and [11], as shown in Table III.

In the second stage, four additional alternatives were analyzed, arising from the planar geometry and readjustment of the original structure, as shown in Table IV.

The two groups of scenarios considered in the study have specific characteristics in terms of aspect ratio and increase in the number of panels tested. The first group is based on the design recommendations shown in [20] and [21], maintaining the h/L ratio between 0,3 and 0,5, with two spans. The second group consists of panels with an aspect ratio between 0,38 and 0,80, with the number of panels increased from 10 to 15, distributed across the desripper. This group includes a configuration without panels but involving a 25 cm reduction in the size of the inlet spillway to the left desanding chamber; this alternative is intended for immediate implementation in the actual structure, considering that the operation of the hydroelectric power plant does not allow for long periods of downtime for maintenance.

TABLE III
SUBMERGED PANELS DIMENSIONS AND UBICATIONS

Alternative	Dimensions	Plan view	Ubication (panel center)
1. Flat (Odgaard, 2009)	h = 0,8 m L = 2,4 m Thickness = 0,15 m α = 20 °		Panel 1 x = 48,18 y = 26,43 Panel 2 x = 48,34 y = 22,93
2. Broken (Barani & Sardo, 2013)	h = 0,8 m L = 2,4 m Thickness = 0,15 m	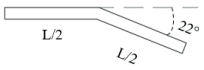	Panel 1 x = 48,31 y = 26,83 Panel 2 x = 48,25 y = 23,20
3. Curved (Barani & Sardo, 2013)	h = 0,8 m L = 2,4 m Thickness = 0,15 m	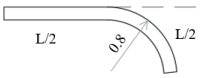	Panel 1 x = 48,31 y = 26,83 Panel 2 x = 48,25 y = 23,20

h = panel height (m); L = panel length (m); α = attack angle (°)

III. RESULTS AND DISCUSSION

Although the results of a three-dimensional numerical model allow for in-depth analysis of the hydrodynamic variables present, the primary objective of this study was to use a validated CFD model to evaluate the alternatives that can be considered to optimize the operation of the desripper and, consequently, the desanding. In this regard, the evaluation of results adheres to the objective of flow distribution in both chambers and, qualitatively, the study of the streamlines generated for each alternative tested.

Fig. 9 shows velocity distribution and streamlines in plan view for the scenarios with flat (b), broken (c), and curved (d) panels, compared to the scenario without panels or validation (a). In the scenario without panels, a greater concentration and velocity of flow was observed towards the right chamber of the desander than towards the left chamber. Additionally, a large counterclockwise recirculation zone was identified upstream of the entrance to the left chamber, which limits the direction of the streamlines and flow velocity towards this chamber. These differences caused an unequal distribution of flow rates in the desanding chambers: 42,67 % to the left chamber (Q_{left}) =5,51 m^3/s) and 57,33 % to the right chamber (Q_{right}) = 7,41 m^3/s).

In general, in the cases with submerged panels (Fig. 9b, 9c, and 9d), changes were observed in the streamlines upstream of the inlet to the desanding chambers, with a slight improvement in the displacement of the main recirculation zone to the left, although new recirculation zones appeared in the right chamber in all cases. The two flat panels option showed, overall, better velocity distribution and displacement of the recirculation zone compared to the broken and curved panels, although these differences had only a marginal impact on flow distribution, as shown in Table V.

Based on the results obtained in the scenario with two flat panels, the model behavior was evaluated under an increased number of panels and geometric modifications, both in panel height and in the height of the original inlet weir to the left desanding chamber. In Fig 10c, it can be seen that reducing the inlet weir height to the left chamber (without panels) generates a similar response to that obtained with the inclusion of two panels, regardless of panel geometry. The increase in the number of panels in the desripper has a considerable effect when their height increases from 0,90 to 1,90 m (Fig. 10a and 10b). This configuration can eliminate the recirculation zone almost entirely upstream of the left desanding chamber.

The scenario combining ten panels of $h = 1,90$ m in the screen and a 0,25 m decrease in the inlet weir height to the left desanding chamber (Fig. 10d) produces the best results in both streamlines and flow distribution, obtaining an almost equal ratio in both desanding chambers (Table V). The presence of a recirculation zone on the right margin of the right disanding chamber indicates the need to complement this investigation in the future, seeking improvements to optimize hydrodynamic behavior.

TABLE IV
COMPLEMENTARY SCENARIOS DESCRIPTION

Alternative	Dimensions	Panels' number
4. Densified flat shape with little increase in height	h = 0,9 m L = 2,4 m Thickness = 0,15 m α = 20°	15 distributed in the desripper zone
5. Densified flat shape with considerable increase in height	h = 1,90 m L = 2,4 m Thickness = 0,15 m α = 20°	15 distributed in the desripper zone
6. Reduction of the height of the inlet weir to the left desander	Weir crest elevation minus 0,25 m	No panels
7. Densified flat shape with considerable increase in height + reduction in height of weir inlet to left desanding chamber	h = 1,90 m L = 2,4 m Thickness = 0,15 m α = 20° Weir crest elevation minus 0,25 m	10 distributed in the desripper zone

Regarding the work of [11], which analyzed the effect of submerged panel shapes and arrangements in a physical model through a channel with two curves (90° and 180°), the effect produced by the panels installed in this research —dealing with a 132° curved-wall desripper— is different from the results observed for the 90° curve, where curved and broken panels were found to be more effective than flat panels. In the case of the 180° curve, the results show the same tendency found in this study, since the flat and curved pannels allow greater flow redirection than the broken panels.

Fig. 11 and Fig. 12 provide a general description of the behavior of the current lines in the vicinity of the panels inserted into the desripper. It can be seen that for all scenarios, the flow patterns differ significantly, with high turbulence between panels.

From a geometrical perspective, limitations were identified regarding the application of the criteria and recommendations of [7] for installing submerged panels in curved channels: the length of the outer edge of the scrapper (14,82 m of the curved section plus 7,85 m of the straight section), compared to the proposed panel length (2,4 m), and the recommended longitudinal spacing of 10 to 30 times the the panel height (in this case from 8 to 24 m), made it difficult to form panel rows as recommended in the literature to achieve effective flow control. Thus, in this research both the flow distribution and the local effect of the panels were analyzed.

The scenario with two flat panels (Fig. 13b) led to the greatest change in flow direction (reference arrow), with an average angle of 24° relative to the scenario without panels. Meanwhile, broken and curved panels produced average angles of 17° and 19°, respectively (Fig. 13). For measuring these angles, a geometric modeling tool was required.

TABLE V
FLOW RATE DISTRIBUTION IN DESANDING CHAMBERS

Alternative	LDC-FR		RDC-FR		TFR	
	(m^3/s)	(%)	(m^3/s)	(%)	(m^3/s)	(%)
No panels	5,61	43,09	7,41	56,91	13,02	100,00
1	5,47	42,01	7,55	57,99	13,02	100,00
2	5,46	41,90	7,57	58,10	13,03	100,00
3	5,52	42,23	7,55	57,77	13,07	100,00
4	5,66	43,40	7,38	56,60	13,04	100,00
5	5,91	45,36	7,12	54,64	13,03	100,00
6	5,82	44,56	7,24	55,44	13,06	100,00
7	6,45	49,01	6,71	50,99	13,16	100,00

LDC-FR: Left Desanding Chamber Flow Rate; RDC-FR: Right Desanding Chamber Flow Rate; TFR: Total Flow Rate

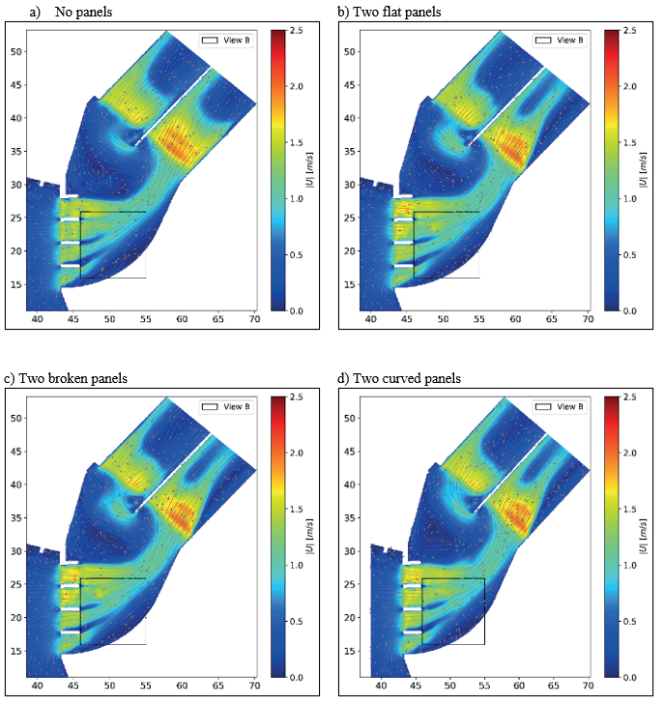

Fig. 9. Plan view velocity distribution and streamlines at desripper and disbanding chambers entrance for panel scenarios with geometry changes: a) no panels, b) two flat panels; c) two broken panels, d) two curved panels.

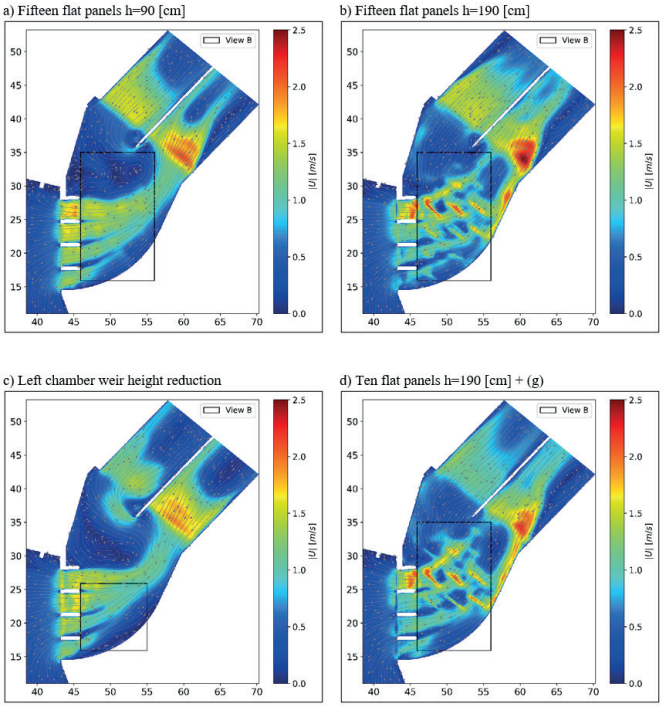

Fig. 10. Plan view velocity distribution and streamlines at desripper and disbanding chambers entrance for scenarios involving an increase in the number of panels: a) fifteen flat panels h = 0,90 m, b) fifteen flat panels h = 1,90 m, c) left chamber weir height reduction, and d) ten flat panels h = 1,90 m + (g).

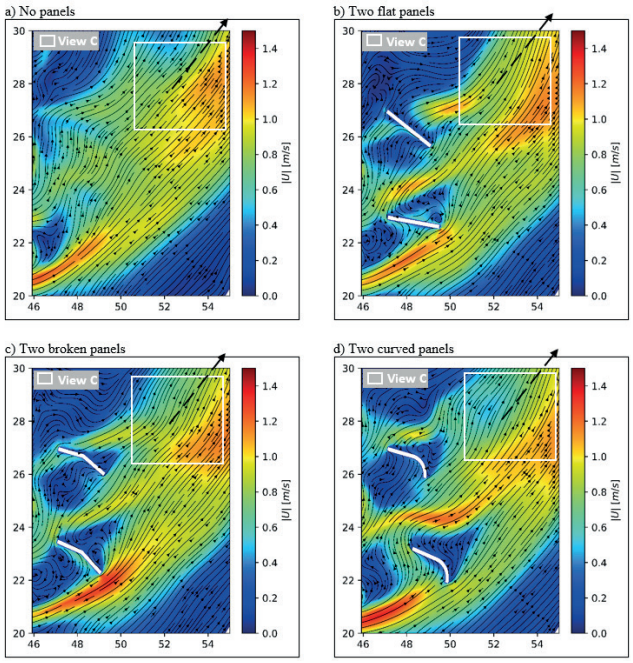

Fig. 11. Plan view (View B) velocity distribution and streamlines at submerged panels zone for panel scenarios with geometry changes: a) no panels, b) two flat panels; c) two broken panels, d) two curved panels.

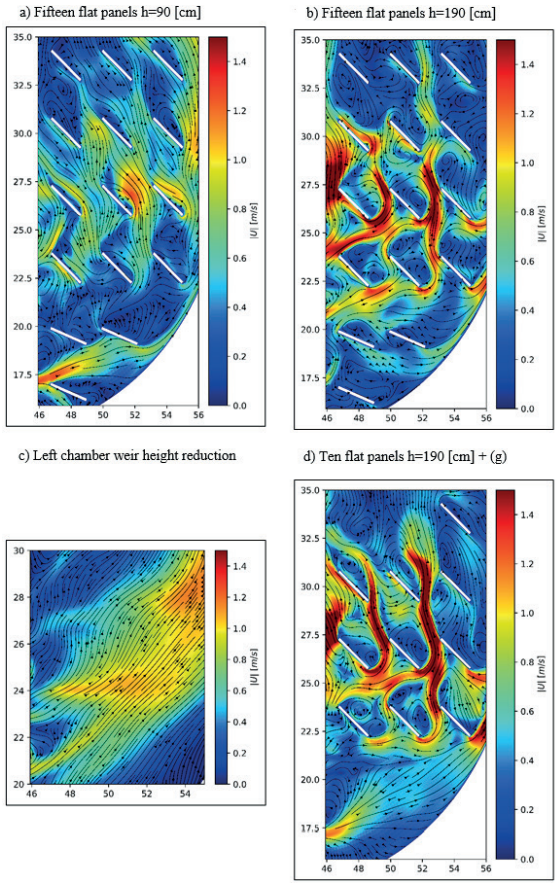

Fig. 12. Plan view (View B) velocity distribution and streamlines at submerged panels zone for scenarios involving an increase in the number of panels: e) fifteen flat panels h = 0,90 m, f) fifteen flat panels h = 1,90 m, g) left chamber weir height reduction and h) ten flat panels h = 1,90 m + (g).

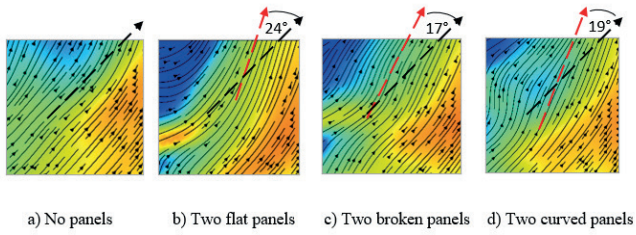

Fig. 13. Plan view (View C) submerged panels influence in flow direction change and diagram of the angle of deflection measured with respect to the scenario without panels; alternatives: a) no panels, b) two flat panels; c) two broken panels, and d) two curved panels

All simulated scenarios involving only the presence of panels do not produce a favorable effect on the equitable distribution of flow to the grit chambers, nor on the recirculation zone that occurs in the left antechamber. This indicates that the design criteria for submerged panels, and even strategies involving increasing the number of panels or aspect ratios, are not directly applicable in curved channels with a small radius of curvature.

The scenario combining an alteration in the control section at the inlet of the left chamber with a densified panel composition and an aspect ratio of 0,8 produces an adequate effect in terms of flow distribution and streamlines in the deflector. This indicates that the problem can be solved by addressing energy dissipation using “deflectors” or “chute blocks”.

IV. CONCLUSION

The model was calibrated, achieving a flow continuity of 96,25 % and a control water depth over the reference weir of 90 % with respect to field data. The model was validated and served as a basis for simplifying the computational domain, optimizing the simulation time of the scenarios with panels.

Seven scenarios were modeled: three with two pairs of submerged panels of different geometric shapes in plan view (flat, broken, and curved) and four with an increased number of flat panels in the desripper and a geometric modification of the inlet weir to the left desanding chamber.

The model without panels (initial condition) shows the presence of a recirculation zone upstream of the left desanding chamber.

The incorporation of two submerged panels, regardless of geometry, does not improve the distribution of flows to the desanding chambers nor substantially modify the recirculation zone, except in the case of curved panels, where a slight displacement of the zone towards the left margin of the screen is observed. Additionally, the submerged panels intensify the velocity field of the wake at the entrance to the left desanding chamber. All these scenarios also generate a new recirculation zone on the right side of the right chamber.

The addition of fifteen submerged panels, combined with an increase in panel height (0,90 m), has a differential effect on flow distribution. However, using the same number of panels with a greater height (1,90 m) almost eliminates the recirculation zone upstream of the left desanding chamber and improves flow distribution to the chambers.

The ten-panel scenario (height 1,90 m) and a 0,25 m reduction in the inlet weir height to the left chamber produced the best results among the evaluated alternatives in terms of equitable flow distribution (49,01 % left; 50,99 % right) and in terms of streamlines, almost eliminating recirculation upstream of the left chamber.

The submerged panels designed based on recommendations in the technical literature did not have a positive influence on eliminating the recirculation zone that causes inadequate flow distribution in the desanding chambers. In this regard, increasing both the number of panels and the aspect ratio —which did have a favorable effect— may contribute to an energy dissipation mechanism in the desripper.

The presence of a recirculation zone on the right bank of the right chamber, present in all scenarios with panels, indicates the need to continue geometric optimization processes to ensure that the hydrodynamic conditions throughout the structure are adequate for the operation of the water intake.

Future work should analyze the effect of other parameters that may influence the performance of submerged panels, such as the angle of attack. In this sense, it is suggested to test the criteria and recommendations of [10], applied to cases of steep and hydraulically tight curves.

ACKNOWLEDGEMENTS

This study is part of the project “Hydrodynamic analysis of the effect of submerged panels in curved channels with fixed bottoms using three-dimensional numerical modeling” (PIIF-22-06), funded by the Escuela Politécnica Nacional (Ecuador). The authors would like to thank the Centro de Investigaciones y Estudios de Ingeniería de los Recursos Hídricos for its collaboration in the use of its facilities and the support of its staff in this study.

REFERENCES

[1] A. Gholami, A. A. Akhtari, Y. Minatour, H. Bonakdari, and A. A. Javadi, “Experimental and Numerical Study on Velocity Fields and Water Surface Profile in a Strongly-Curved 90° Open Channel Bend,” *Engineering Applications of Computational Fluid Mechanics*, vol. 8, pp. 447–461, Dec. 2014, doi: https://doi.org/10.1080/19942060.2014.11015528.

[2] S. Kashyap, G. Constantinescu, C. Rennie, G. Post, and R. Townsend, “Influence of Channel Aspect Ratio and Curvatre on Flow, Secondary Circulation, and Bed Shear Stress in a Rectangular Channe Bend,” *Journal of Hydraulic Engineering*, vol. 128, pp. 1045–1059, Dec. 2012, doi: https://doi.org/10.1061/(ASCE)HY.1943-7900.0000643.

[3] W. van Balen, K. Blanckaert, and W. Uijttewaal, “Analysis of the role of turbulence in curved open-channel flow at different water depths by means of experiments, LES and RANS,” *Journal of Turbulence*, vol. 11, no. 12, 2010.

[4] F. P. García Gutiérrez and J. F. Fernández Bono, “Un método alternativo para estimar la pendiente estable transversal del lecho en canales aluviales curvos,” *Revista Digital Del Cedex*, vol. 69, no. 82, 1992.

[5] S. Kashyap and otros, “Influence of Channel Aspect Ratio and Curvature on Flow, Secondary Circulation, and Bed Shear Stress in a Rectangular Channel Bend,” *Journal of Hydraulic Engineering*, vol. 138, 2012.

[6] L. Olmos, M. Ragessi, C. Pozzi, and C. García, “Estudio Comparativo del Flujo Tridimensional en Canal Curvo con Diferentes Relaciones de Aspecto B/H,” in *XXVII Congreso Latinoamericano de Hidráulica*, 2016.

[7] J. Odgaard, *River Training and Sediment Management with Submerged Vanes*. Texas: ASCE Press, 2009.

[8] B. Taşar, F. Üneş, E. GEMİCİ, M. Demirci, and Y. Kaya, “Numerical Modeling of Submerged Vane Flow.,” Dec. 2023, pp. 111–120. doi: https://doi.org/10.24193/AWC2023_11.

[9] B. Taşar and otros, “Numerical modeling of submerged vane flow,” *Aerul si Apa. Componente ale Mediului*, pp. 111–120, 2023.

[10] A. Voisin and R. D. Townsend, “Model testing of submerged vanes in strongly curved channels,” *Canadian Journal of Civil Engineering*, vol. 29, no. 1, pp. 37-49, 2002.

[11] G. A. Barani and M. S. Sardo, “Experimental Investigation of Submerged Vanes’ Shape effect on river-bend stability,” *Journal of Hydraulic Structures*, vol. 1, no. 1, pp. 35-41, 2013.

[12] T. S. Behbahan, “Laboratory investigation of submerged vane shapes effect on river banks protection,” *Aust J Basic Appl Sci*, vol. 5, no. 12, pp. 1402–1407, 2011.

[13] C. Greenshields, “OpenFOAM v13 User Guide,” 2025, *The OpenFOAM Foundation, London, UK*. Accessed: Dec. 01, 2025. [Online]. Available: https://doc.cfd.direct/openfoam/user-guide-v13

[14] S. Krochin, *Diseño Hidráulico*, Third Edition. Quito: Editorial Escuela Politécnica Nacional, 1986.

[15] Organización Panamericana de la Salud, *Guía para el diseño de desarenadores y sedimentadores*. Lima, Perú: OPS, OMS, Centro Panamericano de Ingeniería Sanitaria y Ciencia, 2005.

[16] N. Olsen, *Computational Fluid Dynamics in Hydraulic and Sedimentation Engineering*. 1999.

[17] H. Imanian and A. Mohammadian, “Numerical simulation of flow over ogee crested spillways under high hydraulic head ratio,” *Engineering Applications of Computational Fluid Mechanics*, vol. 13, no. 1, pp. 983–1000, Jan. 2019, doi: https://doi.org/10.1080/19942060.2019.1661014.

[18] A. Fuentes and otros, “3D modelling of non-uniform and turbulent flow in vertical slot fishways,” *Environmental Modelling & Software*, vol. 99, pp. 156–169, 2018.

[19] D. A. Chin, *Water-Resources Engineering*. New Jersey: Pearson Education, Inc., 2013.

[20] A. J. Odgaard and Y. Wang, “Sediment management with submerged vanes. I: Theory,” *Journal of Hydraulic Engineering*, vol. 117, no. 3, pp. 267 – 283, 1991, doi: https://doi.org/10.1061/(ASCE)0733-9429(1991)117:3(267).

[21] Y. Wang and A. J. Odgaard, “Flow control with vorticity,” *Journal of Hydraulic Research*, vol. 31, no. 4, pp. 549–562, 1993, doi: https://doi.org/10.1080/00221689309498877.